Asymmetric optical properties and bandgap shift of pre-strained flexible ZnO films

Cite as: APL Mater. 12, 041126 (2024); doi: 10.1063/5.0202381
Submitted: 4 February 2024 • Accepted: 9 April 2024 •
Published Online: 24 April 2024

Jiamin Liu,[1] Zhikang Zhou,[1] Honggang Gu,[1] Jinlong Zhu,[1] Hao Jiang,[1] and Shiyuan Liu[1,2,b)]

AFFILIATIONS

[1] State Key Laboratory of Intelligent Manufacturing Equipment and Technology, Huazhong University of Science and Technology, Wuhan 430074, China
[2] Optics Valley Laboratory, Wuhan, Hubei 430074, China

[a)] **Author to whom correspondence should be addressed:** hjiang@hust.edu.cn and shyliu@hust.edu.cn

ABSTRACT

Strain engineering has been extensively explored to modulate the various intrinsic properties of flexible inorganic semiconductor films. However, experimental characterization of tensile and compressive strain-induced modulation of optoelectronic properties and their differences has not been easily implemented in flexible inorganic semiconductor films. Herein, the strain-dependent structural, optical, and optoelectronic properties of flexible ZnO films under pre-tensile and pre-compressive strains are systemically investigated by a Mueller matrix ellipsometry-based quantitative characterization method combined with x-ray diffraction and first-principle calculation. With extended prestress-driven deposition processing under bi-direction bending modes, pre-tensile and pre-compressive strains with symmetric magnitudes can be achieved in flexible ZnO films, which allows precise observation of the strain-driven asymmetric modulation of optoelectronic properties. When the applied prestrain varies approximately equally from 0% (baseline) to −0.99% (compression) and 1.07% (tensility), respectively, the relative changes for the c-axis lattice constant are 0.0133 and 0.0104 Å, respectively. Meanwhile, the dependence factors of the bandgap energy on the pre-compression and pre-tensile strains were determined as −0.0099 and −0.0156 eV/%, respectively, and the complex refractive index also presents an asymmetric varying trend. With the help of the strain–stress analysis and the first-principle calculation, the intriguing asymmetric strain-optical modulation effect could be attributed to the biaxial strain mechanism and the difference in the deformation potential between the two prestrain modes. These systematic investigation consequences are thus promising as a basis for the booming applications of the flexible inorganic semiconductor ensemble.

I. INTRODUCTION

Strain engineering is showing remarkable prospects for modulating and tailoring the physical and chemical properties of various semiconductor materials or films.[1–7] By introducing strain engineering, the optical,[8,9] electronic,[10,11] magnetic,[12] and surface properties[13,14] of inorganic semiconductor materials can be more sufficiently and autonomously tuned than in a strain-free system. The corresponding modulation mechanisms are usually elucidated in terms of the variations in electronic structure and molecular orbital,[6,7,15,16] which are fundamentally caused by the twist, extension, or contraction of the bonds during the lattice deformation. With abundant research involving first-principle calculation or preparation process analysis demonstrating the above mechanisms' rationality,[6–14,17,18] deliberate performance modulations via strain engineering are becoming a practical way to facilitate the performance of related flexible electronic devices.

Due to their excellent optoelectronic properties,[17,18] including wide bandgap, transparency in the visible light band, good conductivity after doping, and the advantages of easy preparation, low cost, non-toxicity, and good thermal stability,[19] ZnO films have been widely used in various flexible electronic scenes,[20–22] such as organic light-emitting diode (OLED) flexible displays, transparent electrodes of polymer solar cells, and thin film transistors. However, due to the low stiffness and weak high-temperature tolerance of flexible substrates, ZnO films grown on flexible substrates often exhibit apparent mechanical and optical anisotropy,[1,23] making preparing and characterizing flexible ZnO films more challenging. Moreover,

flexible ZnO film devices are usually loaded by strain or stress during manufacturing and use,[24] which has a noticeable impact on the optoelectronic properties of ZnO films, thereby affecting the reliability and stability of flexible film devices. Although some studies have reported changes in optical properties such as band gaps and band edges caused by stress or strain, whether anomalous or isolated modulations,[15,23,25–27] rare studies have systematically and experimentally elucidated the stress-optics effect caused by stretching and compression and the difference between these two modes. Therefore, it is of great significance to accurately characterize flexible ZnO films under a series of strain or stress loadings to obtain their photoelectric responses to external mechanical loads.

In fact, there are many studies involving the effects of stretching, bending, and twisting on the bandgap, band edge, and electronic structure of flexible films via first-principles calculations,[28,29] benefiting from the ease of modeling and simulation. On the contrary, experimental observation and verification for the strain dependency of optoelectronic properties in flexible ZnO films might be rare due to the challenges in preparing ZnO films inherently possessing a series of tensile and compressive strains without fracturing and the limitation of readily available optical modeling and measurement techniques.[13,15,23] Thus, it is of great value to accurately characterize the optoelectronic properties of flexible ZnO films that are inherently subject to tensile and compressive strains.

Herein, we propose a Mueller matrix ellipsometry-based quantitative characterization method combined with x-ray diffraction (XRD) and first-principle calculation to systemically investigate the strain-dependent structural, optical, and electronic properties of ZnO thin films deposited on polyethylene terephthalate (PET) substrates. It is possible to prepare flexible ZnO films and load them with tensile and compressive stress without cracking by *in situ* pre-strained PET substrate-based sputtering deposition. Then, XRD was used to determine the crystallographic structural parameters, stress, and strain of the ZnO films, and the first-principles calculation was used to evaluate the effects of tensile and compressive stress on the band structure. A broadband Mueller matrix ellipsometer (MME) has been used to determine the optical constants and their strain-dependent revolution of flexible ZnO films. Experimental and simulation results demonstrated the flexible ZnO films' asymmetric optical and electronic responses to the *in situ* prestrain.

II. METHOD AND EXPERIMENTAL DETAILS

Flexible ZnO films with a nominal thickness of 120 nm were prepared on the *in situ* prestrain-loaded PET substrate by using radio frequency magnetron sputtering (TRP-450, SKY Technology Development Co., Ltd., China) at room temperature, and the entire experimental process was illustrated in Fig. 1(a). Before the deposition of the ZnO thin films, the 170 μm thick PET substrate (DuPont Teijin Films, USA) is cut into 30 × 10 mm^2 rectangular strips. By fixing the ends of the PET strips and compressing one end using a home-built fixture attached with a ruler, as shown in Figs. 1(a) and 1(b), the PET strips were bent upward and downward into sinusoidal shapes, respectively, which would lead to the pre-tensile and pre-compressive strains within the substrate. With the bending curvatures being tuned appropriately, the magnitude of tensile and compressive strains could be adjusted accordingly without any cracking occurring in the PET strips. A group of pre-bent PET strips fixed on the fixture under different bending conditions was put into the sputtering chamber, while another group was released and used for the reference measurement. Then, ZnO films with a nominal average thickness of t_{ZnO} = 120 nm were deposited on the pre-bent PET strips by setting the appropriate sputtering parameters, with

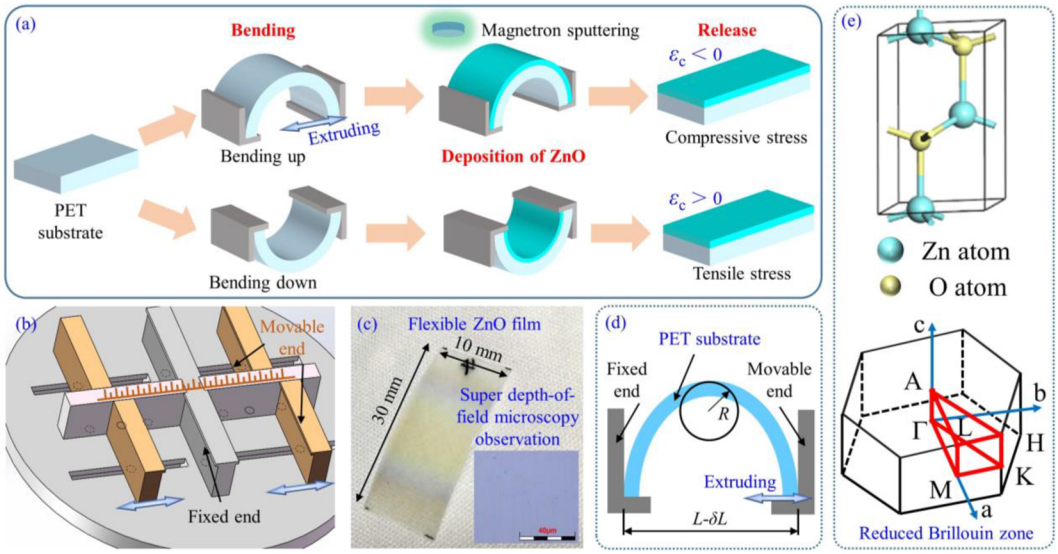

FIG. 1. (a) Schematic processing procedures for preparing *in situ* pre-stretched and pre-compressed ZnO films. (b) Schematic diagram of a home-built fixture attached to a ruler. (c) An exemplary flexible ZnO film subjected to the tensile strain caused by downward bending. (d) Geometrical model of the upward bending. (e) Primitive cell and irreducible Brillouin zone of ZnO crystal.

the growth detailed as demonstrated in the supplementary material. By releasing the samples back to the normal state after maintaining one day of upward bending, the ZnO film is expected to be subjected to uniaxial contraction with residual compressive stress within the sample. While the release after downward bending would induce the uniaxial stretch of the ZnO film, accompanied by residual tensile stress in the sample. Due to the moderate bending, all the ZnO films are intact, and no apparent cracks appear on the sample surface, which was observed by an optical super depth-of-field microscope (DSX 510, Nikon, Japan). Figure 1(c) exhibits an exemplary flexible ZnO film under tensile stress without apparent cracks, demonstrating the high-quality and macroscopically continuous ZnO film grown by the pre-strained deposition. It should be noted that the significant color change at the edge of the ZnO film may be caused by reflection or scattering differences induced by uneven film thickness and surface roughness. Since the adopted probing spots are small enough, usually less than 2 mm, and the film is relatively uniform in the center, the drastic changes in morphology at the edge of the ZnO film will not affect subsequent XRD and MME measurements.

To estimate the strain applied within the ZnO film, a simple-support bending beam model is used to describe the geometric deformation state of the ZnO film,[30,31] as shown in Fig. 1(d). The PET strip with an initial length of L has been compressed to the bent strip with an end-to-end distance of L-δL. Correspondingly, the applied strain ε_a at the surface of ZnO film under upward and downward bending can be evaluated by the derived approximation model, with the derivation details presented in the supplementary material,

$$\varepsilon_{p,up} = \left(\frac{t_{PET}}{2R}\right)\frac{\left[1+2\gamma+0.0167\gamma^2\right]}{[1+\gamma]\cdot[1+0.0167\gamma]},$$
$$\varepsilon_{p,do} = \left(\frac{t_{PET}}{2R}\right)\frac{\left[1+2\eta+60\eta^2\right]}{[1+\eta]\cdot[1+60\eta]}, \quad (1)$$

$$R \approx \frac{L}{2\pi\sqrt{\frac{\delta L}{L}-\frac{\pi^2\cdot t_{PET}{}^2}{12L^2}}}, \quad (2)$$

where $\varepsilon_{p,up}$ and $\varepsilon_{p,do}$ represent the applied strains under the upward and downward bending, respectively. R is the bending radius of the sample. t_{PET} = 170 μm is the thickness of the PET strip. Parameters γ and η satisfy the relationship $\gamma = t_{PET}/t_{ZnO}$ and $\eta = 1/\gamma = t_{ZnO}/t_{PET}$, respectively.

Strain-dependent structural properties of flexible ZnO films were investigated using x-ray diffraction (PANalytical PW3040-60 MRD, Malvern Panalytical, Holland) with Cu $K\alpha$ radiation (λ = 1.5406 Å). All the samples were scanned using $\theta - 2\theta$ mode, with the scanning angle spanning from 30° to 80° and the angle resolution of 0.003°. Based on the Bragg equation,[32] the spacing between the crystal planes could be calculated from the corresponding diffraction peaks, which would support the determination of lattice constants with *a priori* knowledge of hexagonal wurtzite ZnO structure.[33] Then, Mueller matrix spectra of ZnO films and reference PET strips were captured using a commercial Mueller matrix ellipsometer (ME-L, Wuhan Eoptics Technology Co., China) over wavelengths ranging from 250 to 1690 nm.[34,35] To eliminate the back reflection coming from the PET strip's backside, the diameter of the probing spot was reduced to 200 μm using the microspot component, and the substrate's backside surface was fully roughened before the optical characterization. With the ZnO film's dielectric functions parameterized as a polynomial consisting of two Tauc–Lorentz oscillators and an ultraviolet pole term, a stratified optical model based on the parameterized polynomial could be built to fit the measured Mueller matrix spectra of the ZnO films. The multi-incidence measurement mode of the Mueller matrix ellipsometer, with the incidence angle set as 55°, 60°, and 65°, was invoked to suppress the correlations among the fitting parameters. Details involving the fitting analysis can be found in the supplementary material.

The strain-dependency of optical properties for wurtzite ZnO crystals was also investigated using first-principles calculations based on density functional theory with plane-wave pseudopotential.[36] In addition, the exchange–correlation potential was described by the generalized gradient approximations (GAA) with the Perdew–Burke–Ernzerhof (PBE) exchange functional.[37] The primitive cell and the irreducible Brillouin zone of the ZnO crystal with space group $P6_3mc$ for the calculations are presented in Fig. 1(e). Using the convergence test, the sampling strategy for the irreducible Brillouin zone was determined as a 7 × 7 × 7 Monkhorst–Pack grid mesh, and the kinetic energy cutoff was set at 700 eV. By applying uniaxial strains with positive and negative magnitudes along the c-axis, the geometric optimization, the band structure evaluation, and the optoelectronic properties calculation of the strained ZnO crystal were carried out successively, which allows for obtaining the bandgap, the electronic state of density, and the complex refractive index. Details involving the first-principle calculations can be found in the supplementary material.

III. RESULTS AND DISCUSSION

With the *in situ* pre-strained PET substrate-based sputtering deposition shown in Fig. 1(a) being utilized, the applied prestrain ε_p during the upward and downward bending could be tuned by the compressed distance δL according to the above strain model. The corresponding results for δL, R, and ε_p are presented in Table I. No matter whether in the case of upward bending or downward bending, the bending radius R continuously decreases with the compression distance δL increasing, and correspondingly, the applied strain ε_p always increases with the compression distance δL increasing. Due to the non-reciprocity of Young's modulus ratio and thickness ratio for the film and substrate materials in the two bending situations, there will be a slight difference between the magnitude

TABLE I. Applied strain during the bending.

Bending state	Compressed distance δL (mm)	Bending radius R (mm)	Applied prestrain ε_p (%)
Upward bending	10	8.27	1.07
	4	13.08	0.68
No bending	0	∞	0
Downward bending	4	13.08	−0.62
	10	8.27	−0.99

of the tensile and compressive strains caused by the same compression distance. According to the classical mechanics theory,[38] the pre-tensile strain would cause a compressive strain in the ZnO films by releasing after the upward bending, while the pre-compressive strain would lead to a tensile strain in the ZnO films by releasing after the downward bending. For the convenience of elucidation, the positive sign indicates the tensile strain, while the negative sign indicates the compressive strain.

Figure 2(a) shows the XRD patterns of the flexible ZnO films with different applied pre-strains and without prestrains. Except for the one peak from the PET substrate, all films show the (002) and (103) peaks, in which the former peak is much more prominent than that of the latter peak. These results indicate that the high-quality ZnO films grown on the PET substrate have a hexagonal wurtzite structure and are predominantly oriented along the c-axis, perpendicular to the sample plane.[15,39] Moreover, all the (002) peaks located around $2\theta = 34°$ are also similar to the previous studies,[17,39] except for the pre-compressed films' XRD diffraction patterns, which indicates the reliability of XRD results. Figure 2(b) further shows an enlargement of the $\theta - 2\theta$ scan around the (002) diffraction peak. With the applied prestrain transforming from −0.99% to 1.07%, the position of the (002) peak visibly shrinks from 34.34° to 34.13°. A detailed evolution trend of the (002) diffraction peak with the applied prestrain can be found in the inset of Fig. 2(b). Through the piecewise linear fitting analysis, it can be easily noticed that the linear dependency factors of the diffraction angle on the prestrain in the processes of pre-compression and pre-stretch are −0.0673°/% and −0.0215°/%, respectively. The former factor is 3.13 times larger than the latter, which indicates the giant asymmetry in the response of the ZnO crystal structure to the applied strain.

The essence of the above phenomenon lies in the modulation of the c-axial lattice constant by the applied strain, as shown in Fig. 2(c). More specifically, the increase in compressive strain experienced by the ZnO films causes the c-axial lattice constant c to increase from 5.2304 to 5.2408 Å. While the increase in tensile strain within the ZnO films causes the c-axial lattice constant c to decrease from 5.2304 to 5.2171 Å. Considering that the preferentially orientational c axis represents the out-of-plane direction, it can be inferred that ZnO is subjected to biaxial anisotropic strains, namely, opposite-sign in-plane and out-of-plane strains, as shown in Figs. 2(c) and 2(d). With the pre-tensile strain increasing from 0% to 1.07%, the out-of-plane tensile strain experienced by the ZnO films will increase from 0% to 0.1986%, while the in-plane compressive strain will decrease from 0% to −0.1993%. In contrast with the previous observation, the increase of about 0.99% in the pre-compressive strain leads to a rise of about 0.2541% in the out-of-plane compressive strain and a growth of about 0.2550% in the in-plane tensile strain. Meanwhile, the in-plane stress transitions from tensile to compressive stress as the prestrain changes from a compressive to a tensile state. These results mean that ZnO crystal cells have biaxial anisotropic distortion, fundamentally determined by the anisotropic elastic stiffness tensor properties.[40] Notably, the pre-tensile strain of 1.07% can only induce an in-plane compressive stress of −0.9009 GPa, while the pre-compressive strain of −0.99%

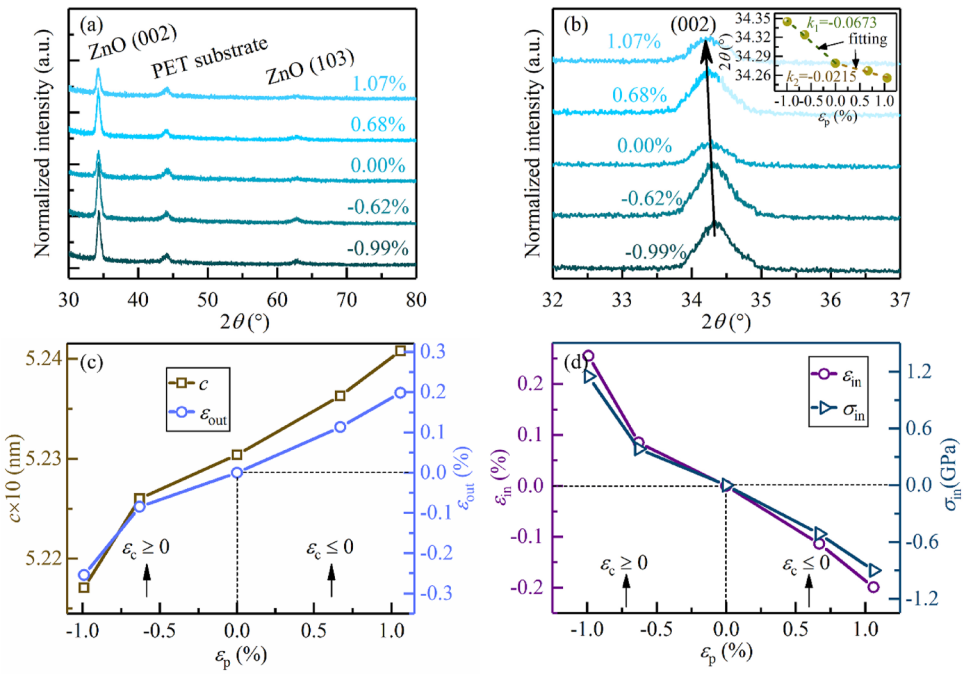

FIG. 2. (a) XRD patterns of flexible ZnO films using the $\theta - 2\theta$ scan from 30° to 80°. (b) Local patterns around the (002) diffraction peaks, with the inset presenting the dependency of the (002) peak on the applied prestrain. (c) Evolutions of the lattice parameter c and out-of-plane strain ε_{out}. (d) Evolutions of the in-plane strain ε_{in} and stress σ_{in}.

can cause an in-plane tensile stress of 1.1526 GPa. This apparent asymmetry might be attributed to the difference between the stretchability and compressibility of the bond lengths in ZnO crystals, which is consistent with the well-known tension–compression asymmetry found in inorganic materials with covalent bonding.[41] That is to say, compressing the spacing between paired atoms in the ZnO lattice cell usually requires more external deformation energy than stretching their spacing. In addition, all the mentioned strains are the applied relative strains, that is, the strain changes between each bending state and the unbending state, rather than the residual strain caused by the sputtering deposition. Considering that all the ZnO films are prepared using the same sputtering deposition process, the residual strains caused purely by the sputtering deposition in all the ZnO films are roughly considered the same. This approximation facilitates revealing the modulation mechanism of applied strain on optoelectronic properties.

With the Debye–Scherrer formula being invoked,[42] the crystallite size of the (002) crystal plane can be extracted from the Gauss-curve-based fitting analysis of the (002) diffraction peaks. Corresponding results are shown in the supplementary material. Compared with the free-strain ZnO crystallite, both the pre-tensile and pre-compression strains will reduce the crystallite size, similar to the strain–grain behavior of ZnO nanoparticles.[43] While both the pre-tensile and pre-compression strains can lead to an increase in both the dislocation density and microstrain. However, these parameters extracted from the fitting analysis only present weak asymmetric but nonmonotonic evolution properties, which indicates that the transition of the external strain state is difficult to cause asymmetry in the crystal nucleation behavior.

Figure 3 exhibits experimental and calculated Mueller matrix elements of an exemplary ZnO film subjected to a pre-compression strain of −0.99%, in which each element spectrum covers a wavelength range of 250–1690 nm. The measured spectra were captured by the Mueller matrix ellipsometry under the incident angle of 65° and the azimuth angle of 0°. In addition, the fitted spectra were reported by the stratified optical model. It can be seen that the flexible ZnO film deposited on the PET substrate exhibits significant optical anisotropy as a whole, which can be evidenced by the occurrence of non-trivial off-diagonal matrix blocks in the Mueller matrix. Considering that ZnO films only have an out-of-plane anisotropic crystalline structure, the observed optical anisotropy mainly originates from the PET substrate, which has been demonstrated by the Mueller matrix measurement of the bare PET substrate.[34] Namely, as the probe light with elliptical polarization enters the PET substrate after transmitting through the isotropic ZnO films, the cross-polarization conversion will occur,[34,44] resulting in non-trivial off-diagonal matrix blocks. Intuitively, the calculated Mueller matrix shows good agreement with the experimental results, accompanied by a mean squared error (MSE) for the fitting regression less than 11. The measured Mueller matrices of other flexible ZnO films can also be well fitted by the stratified optical model, similar to the fitting analysis results shown in Fig. 3. It should be noted that all the thicknesses determined by the MME are average thicknesses due to the introduction of the gravity influence caused by the pre-bending

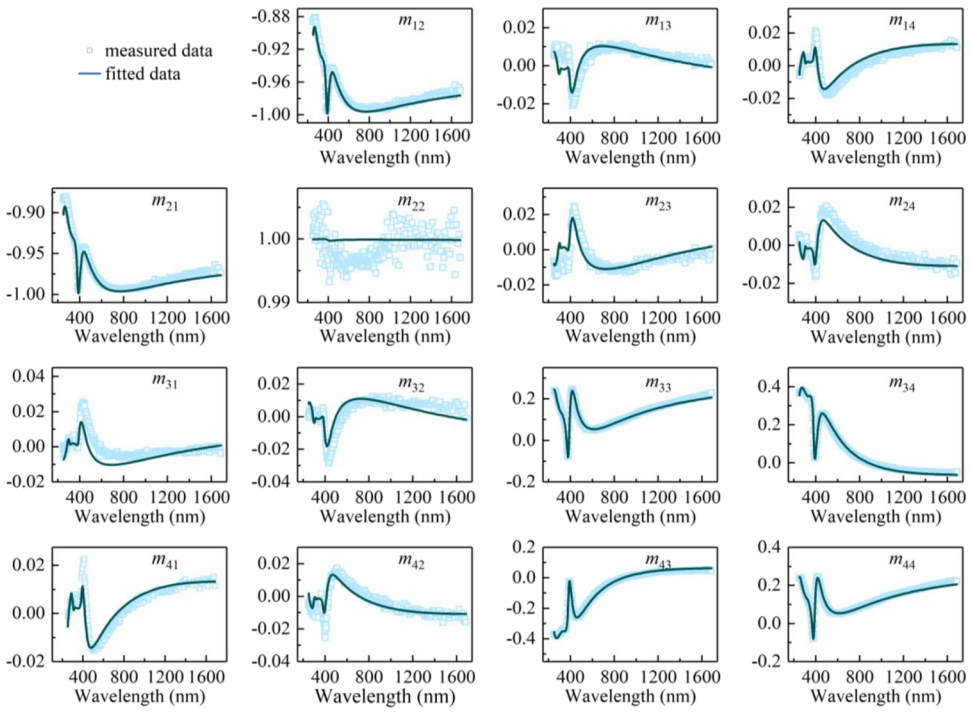

FIG. 3. Mueller matrix elements as a function of wavelength for flexible ZnO film deposited on PET substrate after downward bending. Circles and solid lines represent the experimental and calculated Mueller matrix, respectively.

during the sputtering deposition. The corresponding thicknesses are shown in Table S1 in the supplementary material.

Correspondingly, Fig. 4(a) presents the extracted optical constant of the pre-strained ZnO film, which was quantitatively described by two Tauc–Lorentz oscillators.[42] In the visible and near-infrared regions, the refractive index n gradually decreases with the increase in wavelength, indicating the feature of normal dispersion, while it is opposite in the ultraviolet spectral range. As the extinction coefficient k reveals, the ZnO film exhibits transparency in visible and near-infrared spectra but shows apparent absorption in the ultraviolet range. Figure 4(b) exhibits the evolution of the local complex refractive index spectrum with the applied prestrain ε_p. It can be easily found that both n and k move downward and shift toward shorter wavelengths with the applied prestrain ε_p increasing from −0.99% to 1.07%, especially at the Tauc–Lorentz resonance location. The monotonous evolution indicates an increase in the light propagation speed and penetration capacity within the ZnO films, which are caused by the prestrain-induced modulations. This can be interpreted by the prestress-driven anisotropic deformation of the ZnO lattice.[15,45] Compared with the free-strain case, the out-of-plane tensile strain and the in-plane compression strain induced by the pre-tensile strain can easily lead to a larger lattice constant c and a smaller lattice constant a, which means a more compact arrangement of the in-plane crystal lattice and a stronger in-plane polarization field. The polarization fields usually retard light propagation via the incident light energy loss caused by the dipole alignment,[45,46] and the magnitude of retardation depends on the amplitude of the polarization fields. Accordingly, the light propagation speed in the pre-tensile strained ZnO film is slower than that of the free-strained ZnO film. Meanwhile, the compact arrangement of the in-plane lattice in the semiconductor usually leads to a higher probability of a photon-induced electronic transition, which corresponds to a larger extinction and a smaller penetration depth. As for the pre-compression strain, the effects are precisely the opposite. Moreover, as shown in Fig. 4(b), the modulation effect of the compressive prestrain on the complex refractive index is more prominent than that caused by the tensile prestrain. The origin is still that compressing the spacing between paired atoms along the in-plane direction in the ZnO lattice cell usually requires more external deformation energy than stretching their spacing.

Figure 4(b) presents the Tauc analysis of the absorption coefficient α for the pre-strained ZnO films. Considering that ZnO is a direct-band gap semiconductor, the Tauc relation $(\alpha En)^2 = A(En - Eg)$ between the absorption coefficient α and the bandgap energy Eg has been adopted.[26] Correspondingly, the bandgap energy Eg could be determined by the linear extrapolation of the curve $(\alpha En)^2$ to $En = 0$. The results are shown in Fig. 4(c). By piecewise linear fitting, the dependence factors of the bandgap energy on the pre-compression and pre-tensile strains were determined as −0.0099 and −0.0156 eV/%, respectively. Moreover, the latter dependence factor is nearly 1.5 times that of the former, which intuitively reveals the asymmetric modulation effect of compressive and tensile strains on the bandgap energy of the electronic band structure. Furthermore, the subband gaps and absorption peak locations of the two Tauc–Lorentz oscillators have also been checked, as shown in Figs. 4(e) and 4(f). Indeed, the asymmetric evolutions of the electronic parameters caused by the pre-tensile and pre-compression strains still exist. However, only the bandgap energy Eg_2 for the second Tauc–Lorentz oscillator shows a highly similar evolution trend to the results shown in Fig. 4(d), while the other three electronic parameters exhibit significantly different change trends. The observed similarity seems to imply that the semiconductor's electronic bandgap is determined by the weighted average of the subband gaps of each harmonic oscillator describing the electronic interband transitions. Meanwhile, the strain-dependent evolution characteristics of the transition peaks and subband gaps shown in Figs. 4(e) and 4(f) also indicate that the weighting scheme is challenging to describe analytically and needs further study.

The strain-dependency of the electronic band structure, electronic density-of-states, and the bandgap energy for the polycrystalline ZnO material have been evaluated by the first-principle calculation, as shown in Figs. 5(a)–5(c). Significant bandgap underestimation can be easily found, which is caused by the insufficient accuracy of GAA in describing the exchange–correlation

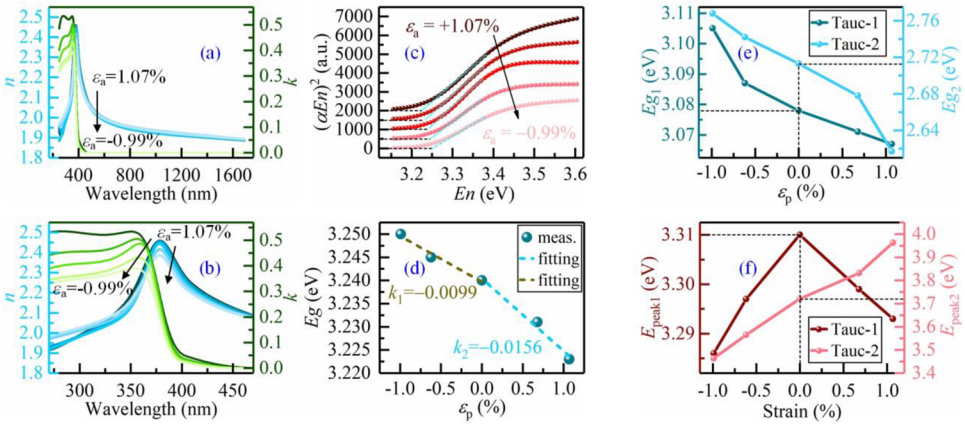

FIG. 4. Optical constants of prestrain loaded ZnO films in the whole (a) and local (b) spectra. (c) Tauc analysis of the absorption coefficient α. (d) Bandgap and its evolution with the prestrain. (e) Bandgaps and (f) peak locations of two Tauc–Lorentz oscillators.

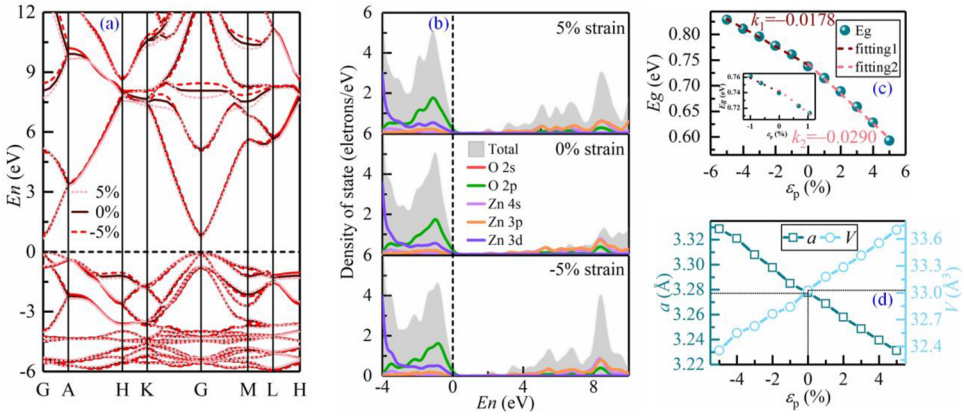

FIG. 5. Calculated band structures (a), electronic density-of-states (b), bandgap energy (c), and the structural parameters (d) of strained ZnO materials. The inserted plot indicates the variation of calculated bandgap energy *Eg* with the applied strain in the range of [−0.99%, 1.07%].

functional.[18,47] However, this calculation error does not affect the analysis of the modulation mechanism of the applied strain on the band structure, density of state, and bandgap energy.[47] Moreover, the utilization of GGA combined with a compelling Coulomb correlation (Ueff) on the d orbital of the Zn atom,[18] the screened hybrid functional theory of HSE,[47] and the many-body GW approach can make the calculated bandgap consistent with the experimental measurement value. However, the computation cost of these techniques is prohibitive, which is not the core of this work. According to the results shown in Fig. 5(a), the applied compression strain can lead to an upward shift of the conduction band minimum (CBM) and a slight downward shift of the valence band maximum (VBM), which further causes the bandgap to broaden. While the tensile strain has the opposite effect. The results shown in Fig. 5(b) also clearly demonstrate the asymmetric modulation effects of compressive and tensile strains on the electronic density-of-states; namely, tensile strain causes an increase in the localization of valence band electrons, and compressive strain leads to an increase in the localization of conduction band electrons. The electronic density-of-states near the CBM shifts slightly toward higher energy levels, accompanied by the upward peak shift of the O 2p states near the VBM as the strain increases from 5% to −5%. These observations support the strain-dependent evolution of the bandgap energy shown in Fig. 5(c). It is easily found that the applied compression strain can lead to in-plane tensile stress, followed by the biaxial strain model, which results in an increasing trend of bandgap with the increasing in-plane tensile stress. While the applied stretching strain can cause in-plane compression stress, which enables the shrinking of the bandgap with the increasing in-plane tensile stress. By piecewise linear fitting, the dependence factors of the bandgap energy on the compression and tensile strains were determined as −0.0178 and −0.0290 eV/%, respectively. Moreover, the latter dependence factor is nearly 1.6 times that of the former, which is highly similar to the strain dependency of bandgap energy revealed by the Mueller matrix ellipsometric experiments. When checking the evolution of bandgap energy *Eg* with the applied strain ε_p in the interval of [−0.99%, 1.07%], the similarly asymmetric modulation effect of strains on the bandgap energy could still be found. Indeed, the goodness of the piecewise linear fitting will be slightly worse, which may be caused by the uncertainty of first-principles calculations in calculating the bandgap modulation effect of small strains. This is why we calculated the strain-dependent bandgap in the large interval [−5%, 5%]; that is to say, the first principle calculation is trustworthy in calculating the evolution trend of physical properties in an extensive range.

Although the measured thickness of the ZnO film varies in an interval [90 nm, 120 nm] as shown in Table S1 in the supplementary material, the bandgap energy evolution shown in Figs. 4(d) and 5(c) is always attributed to the modulation effect of strain rather than the modulation effect of thickness. Without loss of generality, when the thickness of the ZnO film is greater than 20 nm, the complex dielectric function tends to converge to that of the bulk material.[48] While a thinner thickness of less than 20 nm could induce excitonic confinement and exciton localization effects, resulting in thickness-dependent bandgap energy. Meanwhile, with the film thickness exceeding 80 nm, the bandgap energy of ZnO almost does not change.[49] These reported results firmly support the modulation mechanism of strain on the optical properties and bandgap energy in our work. In addition, the first-principle calculations were carried out on the ZnO crystal, which completely shielded the influence of thickness. Thus, the calculated results mainly reveal the influence of applied strain on the band structure, bandgap energy, density of states, etc. Similar calculation results for ZnO nanowires and wurtzite ZnO were reported in Refs. 18 and 47, except for the main focus on the evolution characteristics of the bandgap with strain, which also supports the experimental and theoretical observations in this work.

Furthermore, the observed asymmetric modulation effects of strains on the bandgap energy could be attributed to the anisotropic distortion of the crystal structure, as shown in Fig. 5(d). The anisotropically monotonic evolution of the in-plane lattice constant *a* and the unit cell volume *V* indicates the anisotropic deformation along the out-of-plane and in-plane directions, which further leads to the asymmetry in the deformation potential and the dielectric

susceptibility.[50] The new phenomenon and insights presented here, which quantitatively feature the asymmetric modulation effects of compression and tensile strain on the structural parameters, optical constants, and electronic properties, can be worthwhile for the optimization design and application of ZnO-based flexible electronic devices. In particular, if combining the asymmetric strain-optical modulation effect with the size effect, such as shrinking ZnO from film morphology to a low-dimensional state,[18] the weak asymmetric modulation response described above is expected to be significantly enhanced. It is expected to fabricate flexible biosensors that can sense pulse patterns in the human aorta or force sensors that can realize real-time monitoring of high-rise buildings' stress status.

IV. CONCLUSION

Strain modulation of optical and electronic properties for flexible ZnO films has been systematically demonstrated using an *in situ* prestrain sputtering process and the Mueller matrix ellipsometry-based quantitative characterization method combined with XRD measurement and first-principle calculation. By manipulating the bending curvature of the PET substrate during the *in situ* deposition of flexible ZnO films, tunable pre-compression and pre-tensile strain were deliberately imposed in ZnO thin films with hexagonal wurtzite structure, as evidently confirmed by the XRD characterization. With the applied prestrain changing from −0.99% to 1.07%, the pre-compression strain can cause more significant changes in crystal structure and in-plane stress than the pre-stretching strain with equal magnitude. Similar asymmetric evolutions have also occurred in the measured optical and electronic properties, such as the complex refractive index and the bandgap. By piecewise linear fitting, the dependence factors of the bandgap energy on the pre-compression and pre-tensile strains were determined as −0.0099 and −0.0156 eV/%, respectively. Moreover, the latter dependence factor is nearly 1.5 times that of the former, which intuitively reveals the asymmetric modulation effect of compressive and tensile strains on the bandgap energy of the electronic band structure. This asymmetry effect might be caused by the biaxial strain mechanism and the deformation potential difference. Moreover, the evolutions of the theoretical bandgap and optical constants with the applied strain, reported from the first-principle calculations, also confirm the observed asymmetric strain-optical modulation effect. The dependence factors of the bandgap energy on the compression and tensile strains are determined as −0.0178 and −0.0290 eV/%, respectively. The latter dependence factor is nearly 1.6 times that of the former, which is highly similar to the strain dependency of bandgap energy revealed by the Mueller matrix ellipsometric experiments. It can be expected that the presented basic physical knowledge involving the asymmetric strain-optical modulation effect found in flexible inorganic semiconductor films will provide practical guidance and some novel sights for the optimization design and application of ZnO-based flexible electronic devices.

SUPPLEMENTARY MATERIAL

See the supplementary material for a detailed ZnO deposition process, an approximation model for calculating pre-strains, Mueller matrix ellipsometric analysis, first principle calculations, and XRD (002) peak analysis.

ACKNOWLEDGMENTS

This work was funded by the National Natural Science Foundation of China (Grant Nos. 51975232, 52130504, 52305577, and 52205592), the Key Research and Development Plan of Hubei Province (Grant No. 2022BAA013), the Major Program (JD) of Hubei Province (Grant No. 2023BAA008-2), the Innovation Project of Optics Valley Laboratory (Grant No. OVL2023PY003), and the Nationally Funded Postdoctoral Fellow Research Program (Grant No. GZB20230244). The authors would like to thank the technical support from the Experiment Center for Advanced Manufacturing and Technology in the School of Mechanical Science and Engineering at HUST.

AUTHOR DECLARATIONS

Conflict of Interest

The authors have no conflicts to disclose.

Author Contributions

J.L. and Z.Z. contributed equally to this paper.

Jiamin Liu: Conceptualization (equal); Data curation (equal); Formal analysis (equal); Funding acquisition (equal); Investigation (equal); Methodology (equal); Software (equal); Visualization (equal); Writing – original draft (equal); Writing – review & editing (equal). **Zhikang Zhou**: Conceptualization (equal); Data curation (equal); Formal analysis (equal); Investigation (equal); Methodology (equal); Software (equal); Validation (equal); Writing – review & editing (equal). **Honggang Gu**: Formal analysis (equal); Resources (equal); Writing – review & editing (equal). **Jinlong Zhu**: Formal analysis (equal); Resources (equal); Writing – review & editing (equal). **Hao Jiang**: Conceptualization (equal); Funding acquisition (equal); Investigation (equal); Methodology (equal); Supervision (equal); Writing – review & editing (equal). **Shiyuan Liu**: Conceptualization (equal); Funding acquisition (equal); Investigation (equal); Methodology (equal); Project administration (equal); Supervision (equal); Writing – review & editing (equal).

DATA AVAILABILITY

The data that support the findings of this study are available from the corresponding author upon reasonable request.

REFERENCES

[1] Y. S. Jung, H. J. Choi, J. W. Park, and Y. S. Cho, "Anisotropic in-situ stretching-strain engineering of flexible multilayer thin-film nanogenerators with Cu interlayers," Nano Energy **82**, 105690 (2021).

[2] S. Zhang, Y. Hou, S. Li, L. Liu, Z. Zhang, X. Feng, and Q. Li, "Tuning friction to a superlubric state via in-plane straining," Proc. Natl. Acad. Sci. U. S. A. **116**, 24452–24456 (2019).

[3]D. B. Kim, K. S. Jo, S. J. Park, and Y. S. Cho, "Contribution of anisotropic lattice-strain to piezoelectricity and electromechanical power generation of flexible inorganic halide thin films," Adv. Energy Mater. **12**, 2103329 (2022).
[4]C. Lichtensteiger, C.-P. Su, I. Gaponenko, M. Hadjimichael, L. Tovaglieri, P. Paruch, A. Gloter, and J.-M. Triscone, "a domain engineering in $SrRuO_3$ thin films," APL Mater. **11**, 101110 (2023).
[5]X. Jiang, Y. Liu, Y. Zang, Y. Liu, T. Gao, N. Zheng, Z. Gu, Y. Yang, D. Wu, and Y. Nie, "Uniaxial strain induced anisotropic bandgap engineering in freestanding $BiFeO_3$ films," APL Mater. **10**, 091110 (2022).
[6]C. Zhu, X. Niu, Y. Fu, N. Li, C. Hu, Y. Chen, X. He, G. Na, P. Liu, H. Zai, Y. Ge, Y. Lu, X. Ke, Y. Bai, S. Yang, P. Chen, Y. Li, M. Sui, L. Zhang, H. Zhou, and Q. Chen, "Strain engineering in perovskite solar cells and its impacts on carrier dynamics," Nat. Commun. **10**, 815 (2019).
[7]Y. S. Jung, J. W. Park, J. Y. Kim, Y. Park, D. G. Roe, J. Heo, J. H. Cho, and Y. S. Cho, "Ultrahigh photoresponse in strain- and domain-engineered large-scale MoS_2 monolayer films," J. Mater. Chem. A **11**, 17101–17111 (2023).
[8]G. Ni, H. Yang, W. Ji, S. Baeck, C. Toh, J. Ahn, V. M. Pereira, and B. Ozyilmaz, "Tuning optical conductivity of large-scale CVD graphene by strain engineering," Adv. Mater. **26**, 1081–1086 (2014).
[9]H. L. Liu, M. K. Lin, Y. R. Cai, C. K. Tung, and Y. H. Chu, "Strain modulated optical properties in $BiFeO_3$ thin films," Appl. Phys. Lett. **103**, 181907 (2013).
[10]R. Fei and L. Yang, "Strain-engineering the anisotropic electrical conductance of few-layer black phosphorus," Nano Lett. **14**, 2884–2889 (2014).
[11]A. Castellanos-Gomez, R. Roldan, E. Cappelluti, M. Buscema, F. Guinea, H. S. J. van der Zant, and G. A. Steele, "Local strain engineering in atomically thin MoS_2," Nano Lett. **13**, 5361–5366 (2013).
[12]S. Dai, Y. Lu, and P. Wu, "Tuning electronic, magnetic and optical properties of Cr-doped antimonene via biaxial strain engineering," Appl. Surf. Sci. **463**, 492–497 (2019).
[13]S. Yang, F. Liu, C. Wu, and S. Yang, "Tuning surface properties of low dimensional materials via strain engineering," Small **12**, 4028–4047 (2016).
[14]J. Du, Q. Liao, M. Hong, B. Liu, X. Zhang, H. Yu, J. Xiao, L. Gao, F. Gao, Z. Kang, Z. Zhang, and Y. Zhang, "Piezotronic effect on interfacial charge modulation in mixed-dimensional van der Waals heterostructure for ultrasensitive flexible photodetectors," Nano Energy **58**, 85–93 (2019).
[15]H. J. Choi, W. Jang, B. C. Mohanty, Y. S. Jung, A. Soon, and Y. S. Cho, "Origin of prestress-driven optical modulations of flexible ZnO thin films processed in stretching mode," J. Phys. Chem. Lett. **9**, 5934–5939 (2018).
[16]G. G. Naumis, S. Barraza-Lopez, M. Oliva-Leyva, and H. Terrones, "Electronic and optical properties of strained graphene and other strained 2D materials: A review," Rep. Prog. Phys. **80**, 096501 (2017).
[17]Y. Zhao, H. Yang, B. Yang, Z. Liu, and P. Yang, "Effects of uniaxial stress on the electrical structure and optical properties of Al-doped n-type ZnO," Sol. Energy **140**, 21–26 (2016).
[18]W. A. Adeagbo, S. Thomas, S. K. Nayak, A. Ernst, and W. Hergert, "First-principles study of uniaxial strained and bent ZnO wires," Phys. Rev. B **89**, 195135 (2014).
[19]L. Fang, H. Li, X. Ma, Q. Song, and R. Chen, "Optical properties of ultrathin ZnO films fabricated by atomic layer deposition," Appl. Surf. Sci. **527**, 146818 (2020).
[20]D. Y. Yang, S.-M. Lee, W. J. Jang, and K. C. Choi, "Flexible organic light-emitting diodes with ZnS/Ag/ZnO/Ag/WO_3 multilayer electrode as a transparent anode," Org. Electron. **15**, 2468–2475 (2014).
[21]Z. Chen, J. Wang, H. Wu, J. Yang, Y. Wang, J. Zhang, Q. Bao, M. Wang, Z. Ma, W. Tress, and Z. Tang, "A transparent electrode based on solution-processed ZnO for organic optoelectronic devices," Nat. Commun. **13**, 4387 (2022).
[22]W. Wang, K. Li, J. Lan, M. Shen, Z. Wang, X. Feng, H. Yu, K. Chen, J. Li, F. Zhou, L. Lin, P. Zhang, and Y. Li, "CMOS backend-of-line compatible memory array and logic circuitries enabled by high performance atomic layer deposited ZnO thin-film transistor," Nat. Commun. **14**, 6079 (2023).
[23]S. M. Lee, W. Jang, B. C. Mohanty, J. Yoo, J. W. Jang, D. B. Kim, Y. Yi, A. Soon, and Y. S. Cho, "Experimental demonstration of in situ stress-driven optical modulations in flexible semiconducting thin films with enhanced photodetecting capability," Chem. Mater. **30**, 7776–7781 (2018).
[24]Q. Zhang, Y. Wang, R. Tao, H. Torun, J. Xie, Y. Li, C. Fu, J. Luo, Q. Wu, W. P. Ng, R. Binns, and Y. Q. Fu, "Flexible ZnO thin film acoustic wave device for gas flow rate measurement," J. Manuf. Syst. **30**, 095010 (2020).
[25]Q. Yan, P. Rinke, M. Scheffler, and C. G. Van de Walle, "Strain effects in group-III nitrides: Deformation potentials for AlN, GaN, and InN," Appl. Phys. Lett. **95**, 121111 (2009).
[26]Y. Wang, W. Tang, J. Liu, and L. Zhang, "Stress-induced anomalous shift of optical band gap in Ga-doped ZnO thin films: Experimental and first-principles study," Appl. Phys. Lett. **106**, 162101 (2015).
[27]H. R. Choi, S. K. Eswaran, and Y. S. Cho, "Prestress driven improvement in fracture behavior of in situ sputtered zinc oxide thin films on stretched polymer substrates," ACS Appl. Mater. Interfaces **7**, 14654–14659 (2015).
[28]W. Wu, J. Wang, P. Ercius, N. C. Wright, D. M. Leppert-Simenauer, R. A. Burke, M. Dubey, A. M. Dogare, and M. T. Pettes, "Giant mechano-optoelectronic effect in an atomically thin semiconductor," Nano Lett. **18**, 2351–2357 (2018).
[29]Y. Duan, L. Qin, L. Shi, G. Tang, and H. Shi, "Hybrid density functional theory study of band gap tuning in AlN and GaN through equibiaxial strains," Appl. Phys. Lett. **100**, 022104 (2012).
[30]S.-I. Park, J.-H. Ahn, X. Feng, S. Wang, Y. Huang, and J. A. Rogers, "Theoretical and experimental studies of bending of inorganic electronic materials on plastic substrates," Adv. Funct. Mater. **18**, 2673–2684 (2008).
[31]J. L. Ni, X. F. Zhu, Z. L. Pei, J. Gong, C. Sun, and G. P. Zhang, "Comparative investigation of fracture behaviour of aluminium-doped ZnO films on a flexible substrate," J. Phys. D: Appl. Phys. **42**, 175404 (2009).
[32]C. Suryanarayana and M. G. Norton, Practical aspects of X-ray diffraction, *X-Ray Diffraction* (Springer, 1998), pp. 63–94.
[33]N. Abdullayeva, C. T. Altaf, M. Mintas, A. Ozer, M. Sankir, H. Kurt, and N. D. Sankir, "Investigation of strain effects on photoelectrochemical performance of flexible ZnO electrodes," Sci. Rep. **9**, 11006 (2019).
[34]Z. Zhou, H. Jiang, H. Gu, X. Chen, H. Peng, Y. Liao, S. Liu, and X. Xie, "Strain-optical behavior of polyethylene terephthalate film during uniaxial stretching investigated by Mueller matrix ellipsometry," Polymer **182**, 121842 (2019).
[35]J. Liu, W. Gong, L. Li, S. Zhang, J. Zhu, R. Chen, H. Jiang, and S. Liu, "Longitudinal magneto-optical Kerr effect in subwavelength thick ferromagnetic films investigated by Mueller matrix ellipsometry," Opt. Lasers Eng. **171**, 107803 (2023).
[36]S. J. Clark, M. D. Segall, C. J. Pickard, P. J. Hasnip, M. I. J. Probert, K. Refson, and M. C. Payne, "First principles methods using CASTEP," Z. Kristallogr.-Cryst. Mater. **220**, 567–570 (2005).
[37]J. Wróbel, K. J. Kurzydłowski, K. Hummer, G. Kresse, and J. Piechota, "Calculations of ZnO properties using the Heyd-Scuseria-Ernzerhof screened hybrid density functional," Phys. Rev. B **80**, 155124 (2009).
[38]S. T. Thornton and J. B. Marion, in *Classical Dynamics of Particles and Systems*, 5th ed. (Brooke Cole, 2004), pp. 29–78.
[39]T. Guo, G. Dong, F. Gao, Y. Xiao, Q. Chen, and X. Diao, "High performance ZnO:Al films deposited on PET substrates using facing target sputtering," Appl. Surf. Sci. **282**, 467–471 (2013).
[40]T. Prasada Rao, M. C. Santhosh Kumar, S. Anbumozhi Angayarkanni, and M. Ashok, "Effect of stress on optical band gap of ZnO thin films with substrate temperature by spray pyrolysis," J. Alloys Compd. **485**, 413–417 (2009).
[41]Y. Wang, J. Ding, Z. Fan, L. Tian, M. Li, H. Lu, Y. Zhang, E. Ma, J. Li, and Z. Shan, "Tension-compression asymmetry in amorphous silicon," Nat. Mater. **20**, 1371–1377 (2021).
[42]J. Liu, M. Wang, H. Jiang, J. Lin, H. Gu, X. Chen, T. Shi, and S. Liu, "Annealing temperature dependence of optical and structural properties of Cu films," Phys. Rev. B **101**, 014107 (2020).
[43]A. Khorsand Zak, W. H. Abd. Majid, M. E. Abrishami, and R. Yousefi, "X-ray analysis of ZnO nanoparticles by Williamson–Hall and size–strain plot methods," Solid State Sci. **13**, 251–256 (2011).
[44]H. Fujiwara, *Spectroscopic Ellipsometry: Principles and Applications* (John Wiley & Sons Ltd., 2007), pp. 209–246.
[45]H. J. Choi, W. Jang, Y. E. Kim, A. Soon, and Y. S. Cho, "Stretching-driven crystal anisotropy and optical modulations of flexible wide band gap inorganic thin films," ACS Appl. Mater. Interfaces **11**, 41516–41522 (2019).
[46]A. M. Jones, H. Yu, N. J. Ghimire, S. Wu, G. Aivazian, J. S. Ross, B. Zhao, J. Yan, D. G. Mandrus, D. Xiao, W. Yao, and X. Xu, "Optical generation of excitonic valley coherence in monolayer WS_2," Nat. Nanotechnol. **8**, 634–638 (2013).

[47] Y. Wang, W. Tang, J. Zhu, and J. Liu, "Strain induced change of band structure and electron effective mass in wurtzite ZnO: A first-principles study," Comput. Mater. Sci. **99**, 145–149 (2015).
[48] D. Pal, J. Singhal, A. Mathur, A. Singh, S. Dutta, S. Zollner, and S. Chattopadhyay, "Effect of substrates and thickness on optical properties in atomic layer deposition grown ZnO thin films," Appl. Surf. Sci. **421**, 341–348 (2017).
[49] B. Dong and G. Fang, "Effect of thickness on structural, electrical, and optical properties of ZnO:Al films deposited by pulsed laser deposition," J. Appl. Phys. **101**, 033713 (2007).
[50] Z. Liu, C. Menéndez, J. Shenoy, J. N. Hart, C. C. Sorrell, and C. Cazorla, "Strain engineering of oxide thin films for photocatalytic applications," Nano Energy **72**, 104732 (2020).

Supplementary Material

Asymmetric optical properties and bandgap shift of prestrained flexible ZnO films

Jiamin Liu[1, #], Zhikang Zhou[1, #], Honggang Gu[1], Jinlong Zhu[1], Hao Jiang[1, *], and Shiyuan Liu[1, 2, *]

[1] State Key Laboratory of Intelligent Manufacturing Equipment and Technology, Huazhong University of Science and Technology, Wuhan 430074, China

[2]Optics Valley Laboratory, Hubei 430074, China

[#] These authors contribute equally

[*] Authors to whom correspondence should be addressed: Hao Jiang, hjiang@hust.edu.cn; Shiyuan Liu, shyliu@hust.edu.cn

ZnO deposition growth process

High-quality and continuous flexible ZnO films subjected to different prestrains were prepared by radiofrequency magnetron sputtering (TRP-450, SKY Technology Development Co., Ltd, China) at room temperature. Before bending and sputtering, all the PET substrates were pre-processed to clean the surface. First, the backside faces of all the PET substrates were roughened to reduce back reflection. Then, before the bending, the PET substrates were ultrasonically cleaned with acetone and ethanol for 15 minutes, respectively. Subsequently, the PET substrates were rained with deionized water and dried with nitrogen flow. At last, these dried PET substrates were placed into a vacuum dryer and dried under 40°C for 24 hours. These pre-treatment are necessary to ensure the quality of subsequent ZnO film growth. The magnetron sputtering process begins from putting a group of pre-bent PET strips into the sputtering chamber. During the deposition, the distance between the center of the bent substrate and the ZnO ceramic target with a purity of 99.99% was kept at 10 cm, and the base and work pressure were 2×10^{-3} Pa and 0.6 Pa, respectively. The sputtering temperature was set at 300 K, and the sputtering atmosphere was Ar gas with a purity of 99.999% and injection rate of 65 sccm. Since the sputtering power and the rotation speed of the stage were set at 100 W and 10 rp/min, respectively, a relatively homogeneous deposition rate of ZnO could be estimated at 0.03 nm/sec. Before the growth of ZnO films, the ceramic target was pre-sputtered for 10 minutes to remove the impurity atoms on the target surface. After the sputtering deposition of 60 minutes, the samples remained bent for 24 hours to stabilize the strain state inside the ZnO films. By releasing the samples back to the normal state, the ZnO films are expected to be subjected to uniaxial stretch (contraction) with the residual tensile (compressive) stress in the interior of the samples.

Approximation model for calculating pre-strains

As mentioned in the manuscript, the magnitude of applied strain was tuned by altering the bending curvature radius *R*, which could be determined by the compressive length of the PET stripes. The corresponding diagram of the pre-bending strain loading based on the home-built fixture attached with a ruler is shown in Figure S1.

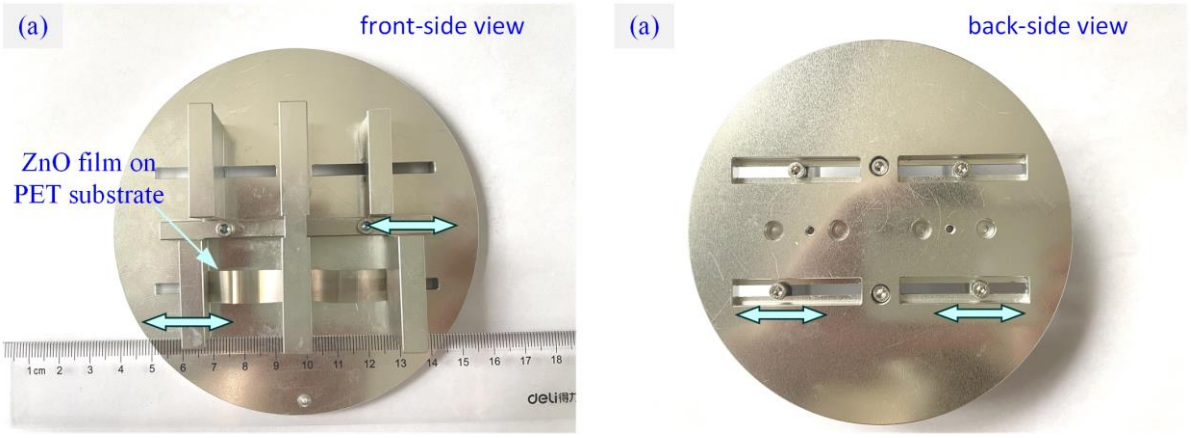

Fig. S1. Schematic diagram of the pre-bending strain loading based on the home-built fixture attached with a ruler.

The PET stripe with an initial length of *L* has been compressed to the bent stripe with the end-to-end distance of *L*-*δL*. Correspondingly, the bending radius *R* could be obtained by the below formula,[1-2]

$$R = \frac{L}{2\pi\sqrt{\frac{\delta L}{L} - \frac{\pi^2 \cdot \left(t_{PET} + t_{ZnO}\right)^2}{12L^2}}}, \tag{S1}$$

where t_{PET} and t_{ZnO} are the thicknesses of the PET stripe and the ZnO film, respectively.

Further, the applied strain εa at the surface of samples can be defined as the following formula,[3]

$$\varepsilon_a = \left(\frac{t_{PET} + t_{ZnO}}{2R}\right)\frac{\left(1 + 2\eta + \chi\eta^2\right)}{(1+\eta)(1+\chi\eta)}, \tag{S2}$$

where $\eta = t_{PET}/t_{ZnO}$ and $\chi = E_{PET}/E_{ZnO}$ for the substrate being bent upward, and $\eta = t_{ZnO}/t_{PET}$ and $\chi = E_{ZnO}/E_{PET}$ for the substrate being bent downward. E_{PET} = 2.5 GPa and E_{ZnO} = 150 GPa are the Young's modulus of the PET stripe and the ZnO film, respectively.[4-5]

Considering that t_{ZnO} = 0.12 μm is three orders of magnitude smaller than t_{PET} = 170 μm and the initial length *L* of the PET stripe is 30 mm, the bending radii *R* for both the upward and downward bending can be simplified as Eq. (S3),

$$R = \frac{L}{2\pi\sqrt{\frac{\delta L}{L} - \frac{\pi^2 \cdot \left(t_{PET} + t_{ZnO}\right)^2}{12L^2}}} \approx \frac{L}{2\pi\sqrt{\frac{\delta L}{L} - \frac{\pi^2 \cdot t_{PET}^{\ 2}}{12L^2}}}, \tag{S3}$$

Correspondingly, the applied strain εa for both the upward and downward bending can be approximated as follows,

$$\varepsilon_{\mathrm{p,\,up}}=\left(\frac{t_{\mathrm{PET}}}{2R}\right)\frac{\left[1+2\left(\frac{t_{\mathrm{PET}}}{t_{\mathrm{ZnO}}}\right)+\frac{1}{60}\left(\frac{t_{\mathrm{PET}}}{t_{\mathrm{ZnO}}}\right)^2\right]}{\left[1+\frac{t_{\mathrm{PET}}}{t_{\mathrm{ZnO}}}\right]\cdot\left[1+\frac{1}{60}\frac{t_{\mathrm{PET}}}{t_{\mathrm{ZnO}}}\right]}\qquad \varepsilon_{\mathrm{p,\,do}}=\left(\frac{t_{\mathrm{PET}}}{2R}\right)\frac{\left[1+2\frac{t_{\mathrm{ZnO}}}{t_{\mathrm{PET}}}+60\left(\frac{t_{\mathrm{ZnO}}}{t_{\mathrm{PET}}}\right)^2\right]}{\left[1+\frac{t_{\mathrm{ZnO}}}{t_{\mathrm{PET}}}\right]\cdot\left[1+60\frac{t_{\mathrm{ZnO}}}{t_{\mathrm{PET}}}\right]}, \tag{S4}$$

Mueller matrix ellipsometric analysis

The measurement and analysis of ZnO samples were carried out using a bottom-up strategy, which includes the measurement and analysis of the PET substrate and the ZnO films deposited on the PET substrate. The results of PET substrates would be used as the input parameters of the stratified optical model in the Mueller matrix analysis of flexible ZnO films. After measuring the Mueller matrix for the bare PET substrate, a stratified optical model based on the transfer matrix method is employed to fit the measurement results,[6-7] which consists of the PET substrate, a roughness layer, and an air ambient layer on the surface of the substrate. In the stratified model, the PET substrate can be considered as a biaxial anisotropic material with its principal optical axis perpendicular to the sample surface. The three diagonal components in its diagonalized dielectric tensor are all described by the Tauc-Lorentz oscillators,[6] and the dielectric response of the roughness layer on the PET substrate is described by a two-phase Bruggeman effective medium approximation (EMA) model.[6] The detailed analysis procedures are similar to the previous work.[6] he optical constants of an exemplary PET substrate without the pre-strain are shown in Fig. S2, in which the apparent anisotropy in optical constants can be attributed to the experience of the biaxially stretching process during preparation. These anisotropic optical constants of the PET substrate are regarded as reference data for the describing the optical constants of flexible ZnO thin film.

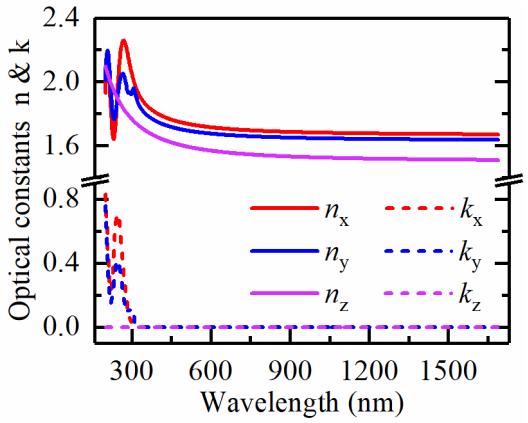

Fig. S2. Anisotropic optical constants of PET substrate as a reference.

Then, another stratified optical model consisting of an air ambient layer, a roughness layer, an isotropic layer, and the above anisotropic substrate layer was used to fit the measured Mueller matrix of flexible ZnO films. Herein, the roughness layer constructed based on the two-phase Bruggeman EMA model describes the dielectric effects of the ZnO films' surface fluctuations,[7] while the isotropic layer corresponds to the flexible ZnO film. In order to determine the thickness of ZnO film, the Cauchy model has been chosen to represent the dielectric functions of the isotropic layer in the spectral range of 500-1690 nm.[7] At this point, the roughness, the thickness, and the coefficients

of the Cauchy model are the fitting parameters in the analysis of the measured Mueller matrix. With the ZnO film's thickness and the roughness being fixed, a B-spline function, as the alternative and extended part of the Cauchy model, has been adapted to describe the dielectric functions in the complete spectral range of 250-1690 nm. Afterward, two Tauc Lorentz oscillators were superposed and utilized to parameterize the B-spline function, which would physically represent the dielectric functions of ZnO film in the entire spectrum.[7] Correspondingly, the figure of merit for the fitting analysis is shown as follows,

$$MSE = \sqrt{\frac{1}{15N - M - 1}\sum_{n=1}^{N}\sum_{i,j=1}^{4}\left[m_{ij,k}^{\exp} - m_{ij,k}^{\mathrm{cal}}\right]^2}, \quad \text{(S1)}$$

where N and M are the number of the wavelength points and the fitting parameters, respectively. $m_{ij,k}^{\exp}$ and $m_{ij,k}^{\mathrm{cal}}$ represent the elements of the measured and the calculated Mueller matrix, respectively.

The optical constants of all the ZnO films subjected to pre-compression and pre-tensile strains are determined according to the above analysis process, and the corresponding results are manifested as the fitting parameters shown in Table S1. The meaning of each coefficient in the Tauc-Lorentz oscillator can be found in Reference [8] and will not be described in detail here. Notably, all the thicknesses presented in Table S1 are the average thicknesses across the entire probing spot of the MME due to the non-flat growing condition and the gravity effect.

Table S1. Fitting parameters of pre-strained ZnO films reported by the Mueller matrix ellipsometry

Applied prestrain	Tauc-Lorentz oscillator								*Average D* (nm)	*Ra* (nm)	*MSE*
	First Tauc-Lorentz oscillator				Second Tauc-Lorentz oscillator						
	A_1	B_1	Eo_1	Eg_1	A_2	B_2	Eo_2	Eg_2			
1.07%	94.270	0.393	3.293	3.067	36.024	3.544	3.962	2.617	116.20	9.51	10.775
0.68%	91.218	0.358	3.299	3.071	32.037	3.282	3.832	2.678	127.01	10.17	10.138
0.00%	84.292	0.326	3.310	3.078	29.694	2.957	3.721	2.713	91.70	7.70	7.779
-0.62%	87.73	0.339	3.297	3.089	31.942	3.472	3.565	2.742	114.53	11.49	7.898
-0.99%	93.099	0.360	3.286	3.105	33.695	3.765	3.464	2.768	105.42	11.16	10.322

First principle Calculations

First-principle calculations were performed for the ZnO primitive cell with hexagonal wurtzite structure using the density functional theory plane-wave pseudopotential method. In the calculations, the exchange-correlation potential was described by the generalized gradient approximations (GAA) with Perdew-Burke-Ernzerhof (PBE) exchange functional based on ultrasoft pseudopotential. The reduced Brillouin zone was sampled with a 7×7×7 Monkhorst–Pack grid mesh, and the kinetic energy cutoff was set at 700 eV, which was usually determined by the convergence test. The convergence tolerances for the maximum force and energy were 0.01 eV/Å and 5×10^{-6} eV/atom, respectively. After the geometric optimization of the primitive cell, the optimized lattice structure has the lattice parameters of a = b = 3.2776 Å and c = 5.2950 Å, which are highly similar to the previous works.[9-14] The deviation between the calculated and the experimental lattice parameters is less than 1%, indicating the rationality and reliability of the simulation results. Then, uniaxial strains were loaded along the c axis of the optimized cell by setting the lattice

parameter *c* as a series of fixed values and keeping both the inplane lattice parameters *a* and *b* as the optimized quantities. Subsequently, the geometric optimization, the band structure, and the optical properties calculations of the strained ZnO crystal were carried out successively to obtain both the band gap and the complex refractive index.

XRD (002) peak analysis

The crystallite size of the (002) crystal plane can be extracted from the Gauss-curve-based fitting analysis of the (002) diffraction peaks. Corresponding results are shown in Table S2.

Table S2 Analysis results for the 002 peaks in the XRD spectra of ZnO films

ε_p (%)	2θ (°)	β (°)	D (nm)	$\delta\times10^3$ (nm^{-2})	$\varepsilon\times10^{-3}$
-0.99	34.3448	0.5817	14.2950	0.0049	8.2
-0.62	34.3238	0.5997	13.8640	0.0052	8.5
0	34.2787	0.5586	14.8827	0.0045	7.9
0.68	34.2671	0.6085	13.6630	0.0054	8.6
1.07	34.2553	0.5831	14.2555	0.0049	8.3

Reference

[1]S.-I. Park, J.-H. Ahn, X. Feng, S. Wang, Y. Huang, and J. A. Rogers, "Theoretical and experimental studies of bending of inorganic electronic materials on plastic substrates," Adv. Funct. Mater. **18** 2673-2684 (2008).

[2]J. L. Ni, X. F. Zhu, Z. L. Pei, J. Gong, C. Sun, and G. P. Zhang, "Comparative investigation of fracture behaviour of aluminium-doped ZnO films on a flexible substrate," J. Phys. D: Appl. Phys. **42** 175404 (2009).

[3]H. J. Choi, W. Jang, B. C. Mohanty, Y. S. Jung, A. Soon, and Y. S. Cho, "Origin of prestress-driven optical modulations of flexible ZnO thin films processed in stretching mode," J. Phys. Chem. Lett. **9** 5934-5939 (2018).

[4]S. Yao, D. Hu, Z. Xi, T. Liu, Z. Xu, and L. Zhao, "Effect of crystallization on tensile mechanical properties of PET foam: experiment and model prediction," Polym. Test. **90** 106649 (2020).

[5]R. Navamathavan, K.-K. Kim, D.-K. Hwang, S.-J. Park, J.-H. Hahn, T. G. Lee, and G.-S. Kim, "A nanoindentation study of the mechanical properties of ZnO thin films on (0 0 0 1) sapphire," Appl. Surf. Sci. **253** 464-467 (2006).

[6]Z. Zhou, H. Jiang, H. Gu, X. Chen, H. Peng, Y. Liao, S. Liu, and X. Xie, "Strain-optical behavior of polyethylene terephthalate film during uniaxial stretching investigated by Mueller matrix ellipsometry," Polymer **182** 121842 (2019).

[7]H. Fujiwara, *Spectroscopic Ellipsometry: Principles and Applications* (John Wiley, 2007), pp. 147-204.

[8]J. Liu, M. Wang, H. Jiang, J. Lin, H. Gu, X. Chen, T. Shi, and S. Liu, "Annealing temperature dependence of optical and structural properties of Cu films," Phys. Rev. B **101** 014107 (2020).

[9]S. K. Yadav, T. Sadowski, and R. Ramprasad, "Density functional theory study of ZnX (X=O, S, Se, Te) under uniaxial strain," Phys. Rev. B **81** 144120 (2010).

[10]Z. A. Alahmed, and H. Fu, "Polar semiconductor ZnO under inplane tensile strain," Phys. Rev. B **77** 045213 (2008).

[11]A. Schleife, F. Fuchs, J. Furthmuller, and F. Bechstedt, "First-principles study of ground-and excited-state properties of MgO, ZnO, and CdO polymorphs," Phys. Rev. B **73** 245212 (2006).

[12]F. Decremps, F. Datchi, A.M. Saitta, A. Polian, S. Pascarelli, A. Di Cicco, J. P. Itié, and F. Baudelet, "Local structure

of condensed zinc oxide," Phys. Rev. B **68** 104101 (2003).

[13]J. E. Jaffe, and A. C. Hess, "Hartree-Fock study of phase changes in ZnO at high pressure," Phys. Rev. B **48** 7903-7909 (1993).

[14]S. Desgreniers, "High-density phases of ZnO: structural and compressive parameters," Phys. Rev. B **58** 14102-14105 (1998).